Seventh International Symp. on Magnetic Bearings, August 23-25 , 2000, ETH Zurich

LORENTZ FORCE TYPE SELF-BEARING MOTOR

Yohji Okada
Dept. of Mechanical Eng., Ibaraki University, Hitachi, 316-8511 Japan
okada@mech.ibaraki.ac.jp

Hirohide Konishi
Dept. of Mechanical Eng., Ibaraki University, Hitachi, 316-8511 Japan

Hideki Kanebako
Dept. of Mechanical Eng., Ibaraki University, Hitachi, 316-8511 Japan
hideki.kanebako@sankyoseiki.co.jp

Chong-Won Lee
NOVIC, Dept. of Mechanical Eng., KAIST, Science Town, Taejon 305-701 Korea
cwlee@hanbit.kaist.ac.kr

ABSTRACT

A new type of self-bearing motor is proposed. It is intended for a single rotor to have two functions of rotary motor and radial active magnetic bearings. Previously proposed PM type self-bearing motor uses reluctance force which requires relatively thin permanent magnet. Hence it has defects of low efficiency and poor reliability. Nonlinearity of magnetic material causes undesirable coupling effect between the radial two directions. Demagnetization of the thin permanent magnet is serious problem for long term use. This paper introduces a new type of self-bearing motor which uses Lorentz force. The rotor has eight strong permanent magnets on the surface of it. The stator has six concentrated windings. Hence it has merits of good dynamic response, good linearity and high reliability. First, the fundamental principle is introduced how the motor produces rotating torque and radial levitation force. Then separate control capability is theoretically developed. Finally two sets of experimental setup are made which will confirm the principle of this motor. The results show high capability of the proposed motor-bearing functions.

INTRODUCTION

Magnetic bearings have been used gradually for vacuum pump or for high-speed rotor due to their non-contact support capability. However, magnetic bearing system requires a separate driving motor. It has defect of long shaft causing low bending vibration. To overcome this difficulty, a self-bearing motor is developed which has two functions of AC motor and radial magnetic bearings on a single disc. However, it requires a complicated flux distribution in the airgap and the efficiency is not so good [1], [2], [3]. Nonlinearity of magnetic material causes undesirable coupling effect between the radial two directions. Demagnetization of the thin permanent magnet is serious problem for long term use.

This paper introduces a new type of self-bearing motor which uses Lorentz force [4]. The rotor has eight strong permanent magnets on the surface of it. The stator has separate six concentrated windings; one set of coil is giving rotary torque while the other set is giving bearing forces. First, the fundamental principle is introduced how the motor produces linear rotating torque and radial levitation forces. Then separate control capability of rotation and radial position is theoretically developed.

To confirm the proposed theory, two types of experimental setup are made; one is the disc type motor and another is the cylindrical type one. Then the static force and torque of the disc type motor is experimentally measured. Rotating property of the disc type motor is also reported which can run up to 2000 rpm. This motor is not powerful enough. Hence we fabricate the cylindrical type one. It can run up to 3200[rpm] with strong torque.

PRINCIPLE OF DISC TYPE MOTOR

Fundamental principle is introduced using disc type motor.

Principle of Rotation

Schematic drawing of the pair of motor coils and the rotor is shown in Fig. 1. The permanent magnets of the rotor produce eight pole flux in the airgap. When the current of pair of motor coil flows coun-

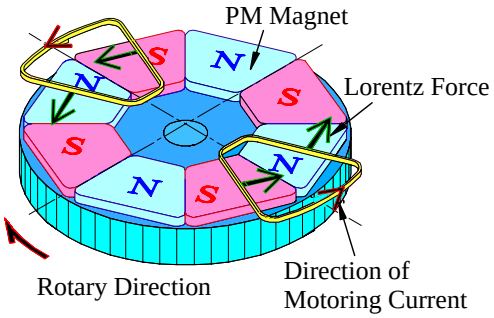

Figure 1: Principle of Giving Rotary Torque

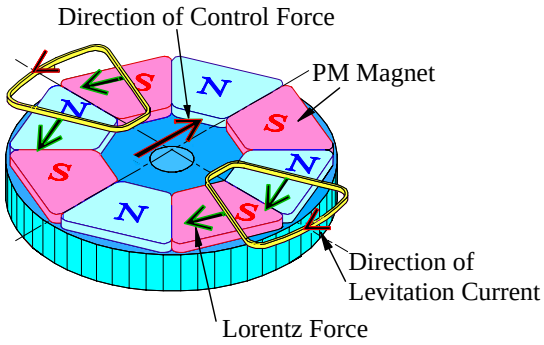

Figure 2: Principle of Giving Bearing Force

terclockwize direction the Lorentz force is produced as shown by the thick arrow in Fig. 1. This reacts to the rotor in the opposite direction to produce rotary torque.

Principle of Bearing Force

The bearing coil is installed in the same place as shown in Fig. 2. Practically one set of coil may be used with the added current of motoring and bearing currents. In this case the currents in the opposite coils are in the opposite direction which cause the radial Lorentz force as shown in Fig. 2.

THEORETICAL CONSIDERATION

The expanded schematic drawing of the rotor and the stator in circumferential direction is shown in Fig. 3. The rotor is written by the eight pole PMs while the stator has two sets of coils. The distance between the going and the returning paths of each concentrated coil is $\frac{\pi}{4}$ apart to produce maximum force and torque which is the same size of rotor permanent magnet. Six coils are wound $\frac{\pi}{3}$ apart and driven by three phase current $U_m, W_m, V_m, U_m, W_m, V_m$ for motoring torque and $U_b, -V_b, W_b, -U_b, V_b, -W_b$ for bearing force, respectively.

Table 1: Definition of Variables

A	Magnitude of motor current
B	Flux density magnitude by permanent magnet
C	Magnitude of levitation current
l	Effective length of coils
r	Radius of rotor
t	Time
θ	Angle
φ	Phase of motor current
ϕ	Phase of levitation current
ω	Electric frequency

Torque control

The rotor is assumed to produce the following flux density.

$$B_g = -B\sin(\omega t + 4\theta) \tag{1}$$

The motor coils are driven by the following three phase current.

$$\begin{aligned} I_{U_m} &= A\cos(\omega t + \varphi) \\ I_{V_m} &= A\cos(\omega t + \frac{2}{3}\pi + \varphi) \\ I_{W_m} &= A\cos(\omega t + \frac{4}{3}\pi + \varphi) \end{aligned} \tag{2}$$

Where the symbols used are listed in Table 1.

The current distribution for half revolution can be written by using Dirac's delta function as follows.

$$\begin{aligned} i_1 &= I_{U_m}\left[\delta(\theta + \frac{\pi}{8}) - \delta(\theta - \frac{\pi}{8})\right] \\ &+ I_{W_m}\left[\delta(\theta - \frac{5}{24}\pi) - \delta(\theta - \frac{11}{24}\pi)\right] \\ &+ I_{V_m}\left[\delta(\theta - \frac{13}{24}\pi) - \delta(\theta - \frac{19}{24}\pi)\right] \end{aligned} \tag{3}$$

The torque produced by this current is calculated using Fleming's left hand rule as follows. Notice that the torque is duplicated by considering the same current from $\frac{7}{8}\pi$ to $\frac{15}{8}\pi$.

$$T = 2rl\int_{-\frac{\pi}{8}}^{\frac{7}{8}\pi} B_g i_1 d\theta = 6rlAB\cos\varphi \tag{4}$$

This solution indicates that the torque is constant and independent from the rotor angle and time. Also this motor can be controlled as the same of the standard PM synchronous motor by the phase φ,

$$\begin{aligned} \varphi = 0° &\Rightarrow \text{Servo motor control by A} \\ \varphi = 90° &\Rightarrow \text{Synchronous motor without load} \\ 90° > \varphi > 0° &\Rightarrow \text{Synchronous motor with load} \end{aligned}$$

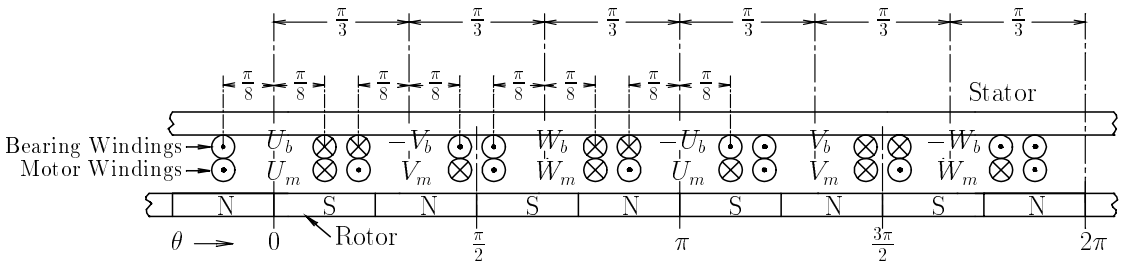

Figure 3: Arrangement of Motor and Bearing Windings

The relation between the electric driving frequency f[Hz] and the rotating speed N[rpm] is ,

$$f = 4 \cdot \frac{N}{60} \quad [\mathrm{Hz}]$$

Bearing force control

The bearing coils are driven by the following current.

$$\begin{aligned} I_{U_b} &= C\cos(\omega t + \phi) \\ I_{V_b} &= C\cos(\omega t + \frac{2}{3}\pi + \phi) \\ I_{W_b} &= C\cos(\omega t + \frac{4}{3}\pi + \phi) \end{aligned} \tag{5}$$

The current distribution is also written using Dirac's delta function as,

$$\begin{aligned} i_2 &= I_{U_b}\left[\delta(\theta+\frac{\pi}{8}) - \delta(\theta-\frac{\pi}{8}) \right. \\ &\qquad \left. -\delta(\theta-\frac{7}{8}\pi) - \delta(\theta-\frac{9}{8}\pi)\right] \\ &+ I_{W_b}\left[-\delta(\theta-\frac{5}{24}\pi) + \delta(\theta-\frac{11}{24}\pi) \right. \\ &\qquad \left. +\delta(\theta-\frac{29}{24}\pi) - \delta(\theta-\frac{35}{24}\pi)\right] \\ &+ I_{V_b}\left[\delta(\theta-\frac{13}{24}\pi) - \delta(\theta-\frac{19}{24}\pi) \right. \\ &\qquad \left. -\delta(\theta-\frac{37}{24}\pi) + \delta(\theta-\frac{43}{24}\pi)\right] \end{aligned} \tag{6}$$

This current produces the radial forces in x and y directions as follows.

$$F_y = l\int_{-\frac{1}{8}\pi}^{\frac{15}{8}\pi} B_g i_2 \cos\theta d\theta = \frac{3\sqrt{2+\sqrt{2}}}{2} BlC\cos\phi \tag{7}$$

$$F_x = l\int_{-\frac{1}{8}\pi}^{\frac{15}{8}\pi} B_g i_2 \sin\theta d\theta = -\frac{3\sqrt{2+\sqrt{2}}}{2} BlC\sin\phi \tag{8}$$

Equations (7) and (8) indicate that the bearing forces are constant and independent from motor angle and motoring current. They can be controlled independently by the magnitude C and phase ϕ of the bearing force current.

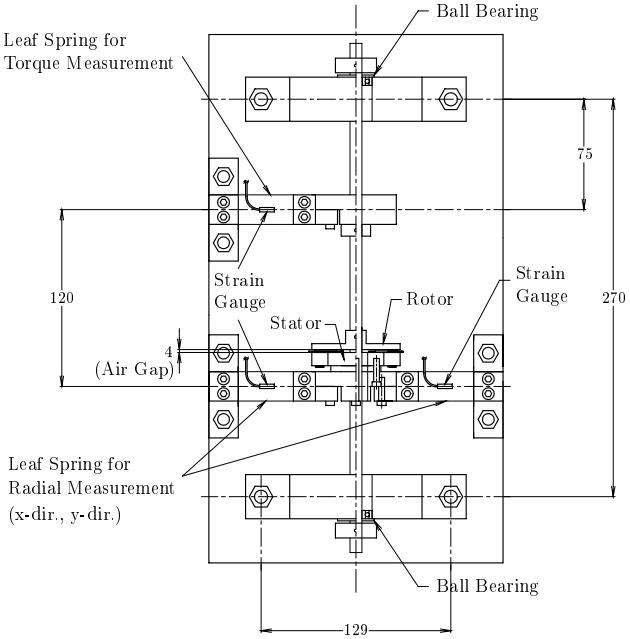

Figure 4: Schematic of Experimental Setup

This motor is 8 pole PM motor which can be controlled by 6 concentrated windings. Hence the efficiency is good due to the low copper loss. Also the dynamic characteristics is very good due to the low inductance and good linearity of Lorentz force.

STATIC FORCE AND TORQUE MEASURMENT

To confirm the proposed theory, a simple experiment is carried out using disc type motor. The static torque and radial force are measured.

Experimental Setup

Schematic of the experimental setup is shown in Fig. 4. The rotor is set vertically. The upper and the lower ends are supported by ball bearings. Hence it has only rotating freedom. The stator is set in the lower part of the rotor which is supported by two

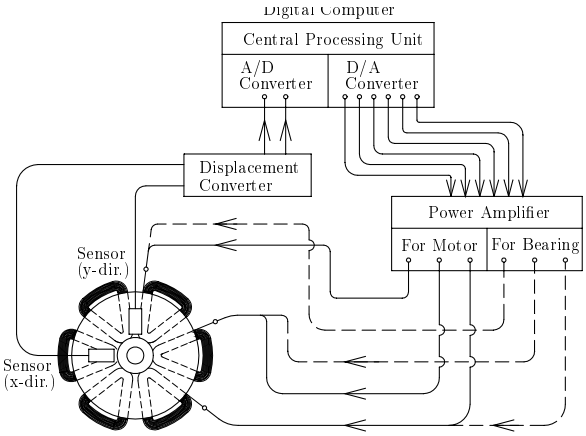

Figure 5: Schematic of Control Systems

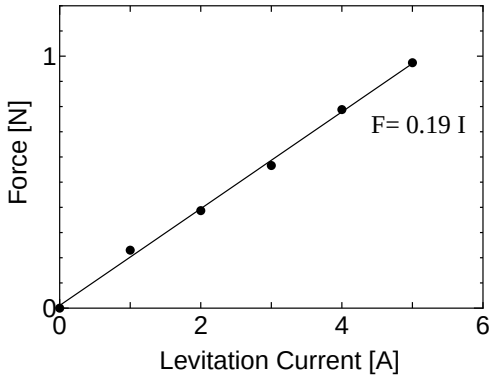

Figure 6: Levitation Force versus Current

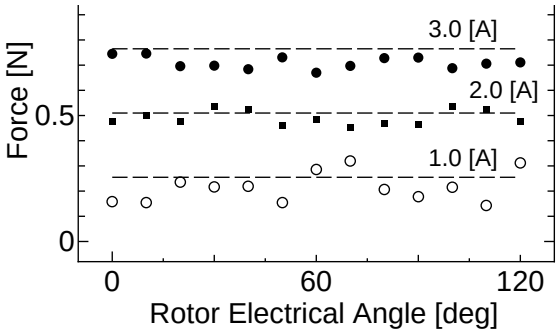

Figure 7: Levitation Force versus Rotor Angle

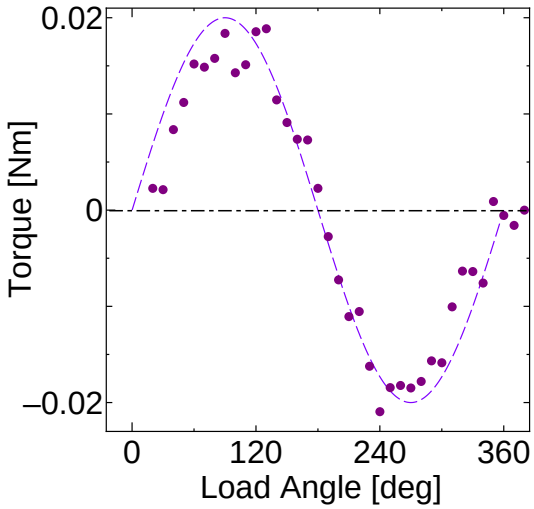

Figure 8: Torque versus Load Angle

leaf springs. The strain gages are glued on them for levitation force measurement. The rotating freedom of the rotor is also restricted by the other leaf spring to measure the produced torque.

Two sets of coils are mounted on the surface of the stator; one for motoring and another for bearing force. Each coil has 22[Turn] with ϕ0.5[mm] wire. The effective length of coil is 15[mm]. Neodymium permanent magnets of 2[mm] thickness are glued on the surface of the rotor which produce maximum gap flux of 0.56[T].

The control system is shown in Fig. 5. The motor and bearing coils are driven by the separate power amplifiers with the maximum current of $\pm$7[A] as shown in the figure. They are controlled by a digital computer (Gateway 2000: P5-60).

Results

The radial force is measured by changing the three phase levitation current from 1[A] to 5[A] as shown in Fig. 6. In this case the rotor angle is fixed and the current phase is set to produce the maximum force. Next the radial force is measured by changing the rotor angle and the current phase synchronously as shown in Fig. 7. In both figures the dots indicate the measured results and the lines are the calculated values. They show relatively good agreement and are not affected by the rotor angle.

The rotating torque is measured by changing the phase φ of the motor current of 7[A]. The results are shown in Fig. 8. The curved lines indicate the calculated values while the dots are the measured results. The measured data have small perturbation, but they agree relatively well with the calculated values.

ROTATING TEST

To confirm the proposed motor the experimental setup is modified and levitated rotation is tested.

Experimental Setup

The modified experimental setup is shown in Fig. 9. The stator and the rotor are the same except the lower end of the rotor is changed free. Hence the rotor has two degrees of freedom in radial x and y directions. The radial displacements are measured by two gap sensors. The axial airgap between the

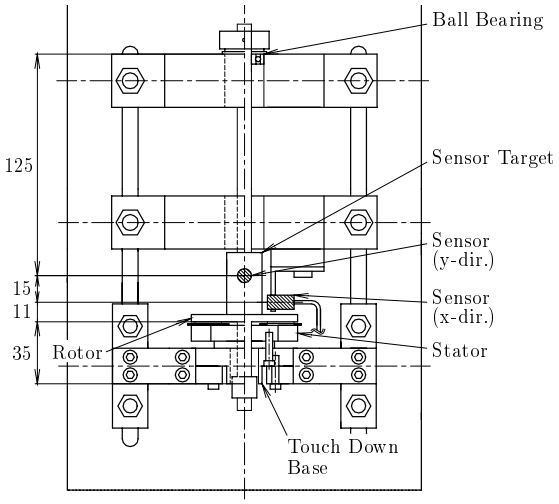

Figure 9: Schematic of Experimental Setup

rotor and the stator is 5[mm]. The equivalent mass of the rotor is 300[g].

Control algorithm

Radial displacements x and y are measured and put into the computer via 12 bit A/D converters. Then the actuating signals are calculated using the standard PID controller for each direction. The controller used is the following discrete PID state equation.

$$\begin{aligned} x_1[k+1] &= x_1[k] + u[k] \\ x_2[k+1] &= e^{-\tau/T_d} x_2[k] + u[k] \\ y[k] &= \tau K_i x_1[k] + \tfrac{K_d}{\tau}(e^{-\tau/T_d} - 1) x_2[k] \\ &+ (K_p + \tfrac{K_d}{\tau}) u[k] \end{aligned} \tag{9}$$

Where the variables are,

$u[k]$	:	input signal to controller
$x_1[k]$	:	state variable for I action
$x_2[k]$	:	state variable for D action
$y[k]$	:	output signal from controller

The magnitude C and phase ϕ of three phase current are calculated from the output signals $y[k] = V_x[k], V_y[k]$ of equation (9) as follows.

$$C = \sqrt{V_x[k]^2 + V_y[k]^2} \tag{10}$$

$$\phi = \tan^{-1}(V_y[k]/V_x[k]) \tag{11}$$

These values are put into Eq. (5). Then each coil current is put out to the power amplifiers via 12 bit D/A converters.

Results

The PID controller is determined experimentally as $K_p = 12$[A/mm], $K_d = 1$[A·sec/mm], $K_i = 5$[A/sec],

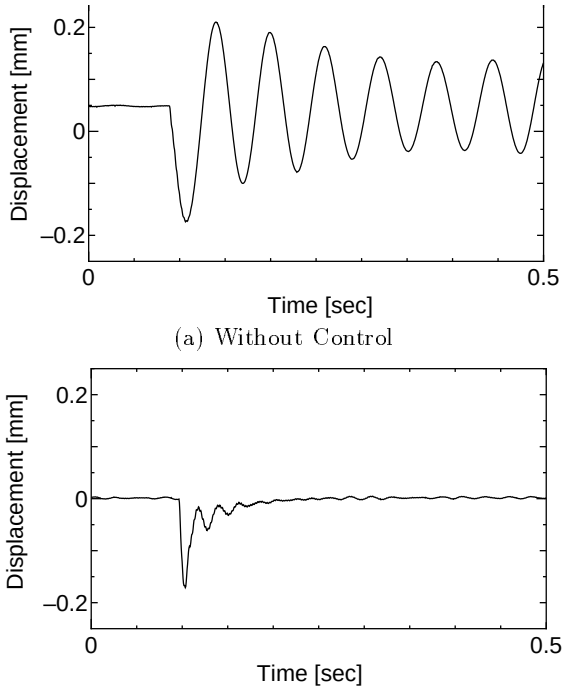

(a) Without Control

(b) PID Control

Figure 10: Impulse Response

$T_d = 9$[msec] and the sampling interval of $\tau = 0.8$ [msec]. Only x directional results are shown in the following figures.

The impulse response is measured by hammering the sensor target and recording the corresponding response as shown in Fig. 10. Where (a) is the response without control and (b) indicates the response with control. Without feedback the system behaves as the pendulum. The stability of it is well improved with PID control.

Next the rotating test is carried out with the motor current of 7[A]. The rotor can run up to 2000[rpm] as shown in Fig. 11, where (a) is the response without feedback and (b) is that with feedback. The rotor is well controlled up to 1800[rpm]. But the response with feedback becomes worse near 2000[rpm] mainly due to the low sampling rate of $\tau = 0.8$[msec].

CYLINDRICAL MOTOR EXPERIMENT

The previous motor is not powerful. Also the radial direction of disc motor is fundamentally stable while that of cylindrical motor is unstable. Hence we developed the powerful cylindrical motor.

Experimental Setup

The schematic of the test motor is shown in Fig. 12. The rotor has the diameter of 54[mm] and the length of 56[mm]. Strong permanent magnets are glued on the surface of rotor which produces the maximum

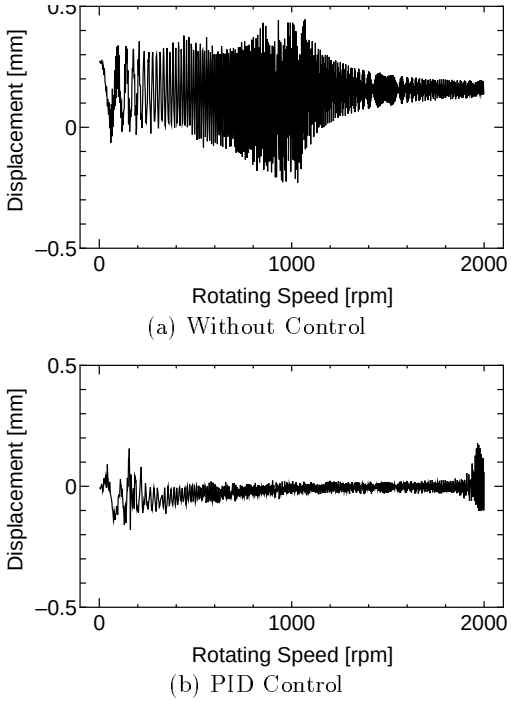

Figure 11: Vibration Amplitude versus Rotating Speed

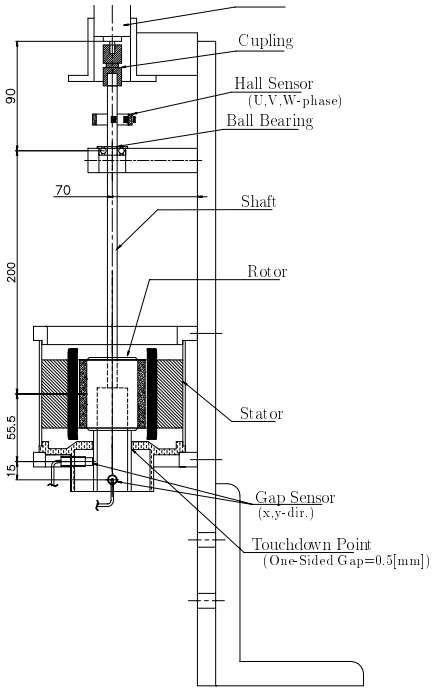

Figure 12: Schematic of Experimental Setup for Cylindrical Motor

flux density of 0.45[T]. The stator has slotless back yoke with laminated sheet. The airgap is 15.5[mm] including PM and 9.5[mm] excluding PM.

The rotation is controlled by a standard three phase inverter based on the measured rotor angle while the levitation is controlled by a DSP (mtt, Lory Accel). The levitation controller is also PID controller with $K_p = 25$[A/mm], $K_d = 0.019$[As/mm], $K_i = 8$[A/smm], $T_d = 0.8$[ms] and $\tau = 0.1$[ms].

Results

The levitated rotating test is carried out and the unbalance response is measured as shown in Fig. 13. The top speed of 3200[rpm] is recorded. This speed limit is mainly due to the bending vibration of the thin shaft at 250[Hz]. The rotating torque is not measured. But we can feel strong torque by grasping the rotating shaft. We are now modifying the experimental setup to get higher rotating speed.

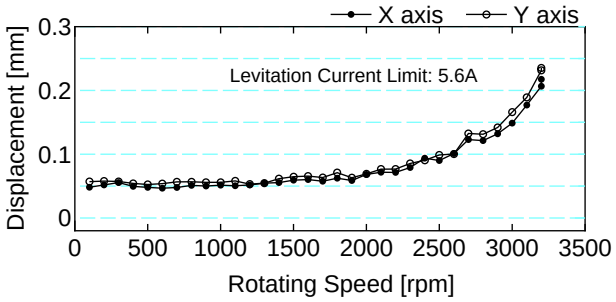

Figure 13: Unbalance Response of the cylindrical motor

CONCLUDING REMARKS

Lorentz force type self-bearing motor is developed. This theory can only be applicable to eight pole motor. But it can be controlled by six concentrated windings. Hence this motor has merits of good efficiency, easy manufacuring and high reliability. Two types of experiment are performed and the results show high capability of this motor. Further work is continuing to improve the laboratory model setup and apply it to the real rotating machinery.

References

[1] A. Chiba, et. al., "An Analysis of Bearingless AC Motors", IEEE Trans. on Energy Conversion, 9-1 (1994), pp. 61–67.

[2] R. Schöb and N. Barletta, "Principle and Application of a Bearingless Slice Motor", Proc. of 5th Symp. on Magnetic Bearings, Kanazawa, Japan, August (1996), pp. 313–318.

[3] Y. Okada, et. al., "Magnetically Levitated Motor for Rotary Blood Pump", Artificial Organs, 21-7 (1997), pp. 739–745.

[4] H. Konishi, et. al., "Development of Lorentz Force Type Selfbearing Motor", Trans. JSME, 66-646C, (2000-6), (will appear soon, in Japanese)